Sensitivity of VOF simulations of the liquid jet breakup to physical and numerical parameters

H. Grosshans [a,e,*], A. Movaghar [b], L. Cao [c], M. Oevermann [b], R.-Z. Szász [a], L. Fuchs [d]

[a] Division of Fluid Mechanics, Lund University, Lund, Sweden
[b] Department of Applied Mechanics, Chalmers University of Technology, Gothenburg, Sweden
[c] Key Laboratory for Aerosol-Cloud-Precipitation of China Meteorological Administration, Nanjing University of Information Science & Technology, Nanjing, China
[d] Department of Mechanics, KTH, Stockholm, Sweden
[e] Institute of Mechanics, Materials and Civil Engineering, Université catholique de Louvain, Louvain-la-Neuve, Belgium

ARTICLE INFO

ABSTRACT

In this paper the characteristics of the primary breakup of a liquid jet is analyzed numerically. We applied the Volumes of Fluids (VOF) approach utilizing the Direction Averaged Curvature (DAC) model, to estimate the interface curvature, and the Direction Averaged Normal (DAN) model, to propagate the interface. While being used for the first time to predict liquid atomization, this methodology showed a high accuracy. The influence of varying the fluid properties, namely liquid-gas density and viscosity ratio, and injection conditions is discussed related to the required grid resolution. Resulting droplet sizes are compared to distributions obtained through the One-Dimensional Turbulence (ODT) model.

1. Introduction

Atomizing liquid jets are frequently occurring in industrial applications. For example, in combustion devices driven by liquid fuel, a fuel jet is injected in the combustion chamber. Before the combustion process takes place, the liquid jet needs to break up into small droplets, evaporate and mix with the surrounding air. The characteristics of the primary breakup of the fuel jet, i.e. liquid breakup length, local droplet diameter or velocity distributions, is crucial for the efficiency and exhaust level of the subsequent combustion process.

Due to its importance, these flows have been analyzed extensively by means of experiments in the last decades. For instance, Hiroyasu and Kadota [29] found an empirical best-fit relation between the fuel injection pressure, the ambient air density, the fuel mass flow rate and the Sauter Mean Diameter (SMD) of the resulting droplet distribution. In the following years Elkotb [9], Varde et al. [76] and Faeth et al. [10] included additionally the effects of liquid viscosity, liquid density and surface tension in the study. Furthermore, Reitz and Bracco [58] derived correlations for the breakup length of the liquid core.

Farth et al. [11] identified the implosion of cavitation bubbles, turbulence in the liquid jet and aerodynamic liquid-gas interaction to be the most dominant mechanisms for liquid jet atomization. Since the first and second mechanisms are related to phenomena occurring inside the injection nozzle, a number of researchers elucidated the influence of the in-nozzle flow on the following jet break-up. For example, Martínez-Martínez et al. [48] reported a high dependence of the spray penetration length on the nozzle diameter. Moreover, Suh and Lee [72] found that an increase in the nozzle length to width ratio enhances the generation of cavitation bubbles in the nozzle and fuel atomization.

Extensive reviews summarizing the knowledge concerning the fundamental aspects of the physics of the disintegration of liquid jets have been provided by Sirignano and Mehring [69] and Eggers and Emmanuel [8].

However, due to the large number of droplets, experimental measurements in these flow regions are very challenging. Especially when looking at droplet size distributions in optically dense sprays, results are blurred due to multi-scattering effects. Aiming to remove these effects, new experimental techniques have been developed in the recent years. Its potential to tackle this problem has been demonstrated by a group of methods based on Structured Laser Illumination Planar Imaging (SLIPI) [3]. A further advancement represents Dual-SLIPI [36] which even proved to be an adequate method to validate numerical models [20,21].

Somewhat similar to SLIPI is an approach called ballistic imaging. However, in ballistic imaging the photons affected by multi-scattering are rejected before the camera, while they are rejected by image processing after the images have been recorded in SLIPI. Ballistic imaging has been used successfully to image the liquid/gas interface of intact liquid structures inside the dense spray region [see the review of Linne [43]].

Despite all experimental effort, the influence of the fluid properties on the liquid jet break-up is not yet fully understood. This is not only due to the optical density but also the full parameter range has not been studied so far. In particular, data concerning the effect of the viscosity of the surrounding gas is rare.

Furthermore, an important disadvantage of experiments is the difficulty to assess isolated effects. For this reason it is difficult to derive conclusions concerning the physics of the flow. For example from the above discussed experimental works it can not be concluded if the influence of the injection conditions on the jet break-up is caused by the changes in the in-nozzle flow, aerodynamic instabilities or something else.

Numerical simulations give the possibility to obtain results of a higher resolution and for isolated effects. The approaches usually applied to simulate sprays include the Eulerian–Eulerian and Lagrangian Particle Tracking (LPT) method. Both assume the liquid phase to be dispersed. The primary breakup of the liquid jet is not resolved, at its best it can be included in the simulation by modeling assumptions.

To simulate the primary breakup the liquid-gas interface is required to be resolved on the numerical grid. Following van Wachem and Schouten [75], methods that resolve the liquid-gas interface can be grouped into surface tracking methods and volume tracking methods. Surface tracking methods include the front tracking [74] and the level-set method [53,64]. These methods solve for the position of the interface while the volume of each phase is reconstructed. Therefore, surface tracking methods suffer in their original formulations from inaccuracies in the volume reconstruction. Also, the liquid volume in the domain is not conserved.

Volume tracking methods are the marker and cell [27] and the Volumes of Fluids (VOF) method [30]. These methods solve for the volume of each phase while the interface is reconstructed. Consequently, volume tracking methods suffer in their original formulations from errors in the interface curvature.

Recent reviews summarizing the available computational models used to describe the atomization of jets were given by Gorokhovski and Herrmann [18] and Jiang et al. [32]. However, all attempts to resolve a strongly curved interface require a very high grid resolution. Therefore, only in the recent years sufficient computational capabilities are available to perform this kind of simulations.

Important implementations include the one by Desjardins et al. [6] and Desjardins and Pitsch [7] who applied a version of level-set which aims to be nearly mass conservative. To handle the high gradients at the liquid-gas interface, they implemented the ghost-fluid method. Furthermore, a combined VOF/level-set method was used by Le Chenadec and Pitsch [38]. To improve the grid quality at the interface they allowed mesh deformations. Fuster et al. [13] utilized the VOF method and improved the grid resolution at the interface, depending on its curvature, applying the octree adaptive grid refinement. A further combination of methods was proposed by Menard et al. [50] who exploited the advantages of each the VOF, level-set and ghost-fluid approach. When compared to experimental data of Diesel injection [39], they recovered well the influence of the surrounding gas temperature. Shinjo and Umemura [65–67] developed a numerical method that applies the level-set method and an improved VOF formulation to combine the benefits of both. They analyzed the isolated aerodynamic breakup effect of a jet injected into still air while the in-nozzle flow was not taken into account. Through computing on a very fine grid (the nozzle diameter was resolved by 285 grid points) they could observe the ligament formation both from the mushroom tip edge and the liquid core surface. The droplet formation occurred from the ligament tip mostly by the short-wave mode.

Some researches aimed to evaluate the influence of the in-nozzle flow on the jet break-up. Som et al. [71] simulated only the nozzle flow solving the RANS (Reynolds Averaged Navier–Stokes) equations. The mass flow at the nozzle exit was analyzed depending on the fuel type, the injection pressure and the needle lift position. The subsequent coupling of RANS simulations of a nozzle flow to a liquid jet was performed by Yuan and Schnerr [80]. They demonstrated the enhancement of atomization due to cavitation by comparing a case applying a cavitation model with a case without. Moreover, recent time resolved Large Eddy Simulations (LES) by Ghiji et al. [16] of the flow inside a simplified nozzle and the subsequent atomization indicated a good agreement with experiments during early stages of Diesel injection. An approach without resolving the in-nozzle flow was recently followed by Xiao et al. [78]. They implemented the Rescaling and Recycling Method to facilitate generation of appropriate unsteady LES inlet conditions. The method was applied to replicate the turbulent nozzle outflow and to investigate its influence on the liquid jet. Siamas et al. [68], on the other hand, focused on evaluating the effect of swirl created inside the nozzle on the flow field of annular gas-liquid jets using detailed VOF simulations. They identified the swirling motion to be responsible for the development of a central recirculation zone.

Besides the above discussed model developments, a new formulation of the VOF approach utilizing the Direction Averaged Curvature (DAC) and Direction Averaged Normal (DAN) models was proposed by Lörstad and Fuchs [47]. However, the method was so far only applied to compute bubbles and not yet to liquid jets. Nevertheless, its accuracy when describing bubbles was intensively tested by Lörstad et al. [45,46]. It was reported to remedy some of the main issues in the VOF method: the DAC model was shown to model the surface tension forces highly accurate for high Reynolds number flows. Furthermore, the DAN model proved to be second-order accurate, mass conservative, without over- or undershoots of the phase variable, and, most important, non-diffusive.

A simplified approach to resolve a turbulent flow, which is worth mentioning, is called One-Dimensional Turbulence (ODT). It has been originally proposed by Kerstein [33] and was extended by Kerstein et al. [34] and Ashurst and Kerstein [2]. The major advantage compared to the above discussed methods lies in its computational efficiency which allows to explore flow regimes (Reynolds and Weber numbers here) which are not accessible by LES or Direct Numerical Simulation (DNS) methods. This methodology was used by Movaghar et al. [51] to study the outcome of liquid atomization. Despite the limitation of the model to simulate topologically simple flows with one dominant flow direction, e.g. simple jets or boundary layers, the method has proven to correctly predict many different scaling laws in turbulent flow.

To sum up, the theoretical research until today focuses mainly on the improvement of the computational methodology. So far only a few investigations focused on gaining physical insight.

In the present study for the first time the VOF/DAC/DAN method was applied to the case of an atomizing liquid jet. In this paper the capabilities of the VOF/DAC/DAN method to accurately model the primary breakup of a liquid jet in relation to the required grid resolution are discussed. The method is utilized to study the influence of the fluid properties, such as liquid-gas density and viscosity ratio, and the injection profiles on the flow. The results are compared to data generated by the ODT model. The comparison is based on the resulting droplet diameter distribution, which is most sensitive to the resolution of the applied grid.

2. Description of the VOF/DAC/DAN approach

The VOF method is used to handle the liquid and the gaseous phase. The flow field is described in an Eulerian framework by the incompressible, isothermal Navier–Stokes equations for multiphase flows without phase changes. The non-dimensional mass and momentum conservation equations are given by

$$\frac{\partial u_i}{\partial x_i} = 0 \tag{1}$$

$$\rho\frac{\partial u_i}{\partial t} + \rho u_j\frac{\partial u_i}{\partial x_j} = -\frac{\partial p}{\partial x_i} + \frac{1}{Re_{\text{jet}}}\frac{\partial}{\partial x_j}\left(\mu\left(\frac{\partial u_i}{\partial x_j}+\frac{\partial u_j}{\partial x_i}\right)\right) + \frac{\kappa\delta n_i}{We_{\text{jet}}}. \tag{2}$$

Herein u_i, p, ρ and μ denote the velocity components, the pressure, the density and the dynamic viscosity of the fluid, respectively. The last term on the right hand side of the momentum equation represents forces due to the surface tension, where δ is a Dirac function which vanishes everywhere except at the interface, κ the interface curvature and n_i the interface unit normal.

In the above equation, the jet Reynolds number, Re_{jet}, and the jet Weber number, We_{jet}, are based on the injection velocity U_{inj} and the nozzle diameter d_{noz}, namely

$$Re_{\text{jet}} = \frac{\rho_l U_{\text{inj}} d_{\text{noz}}}{\mu_l} \quad\text{and}\quad We_{\text{jet}} = \frac{\rho_g U_{\text{inj}}^2 d_{\text{noz}}}{\sigma}. \tag{3}$$

In this equation σ denotes the surface tension and the indices l and g the liquid and the gas phase, respectively. The fluid properties in Eqs. (2) and (3) are calculated linearly dependent on the phase variable α as

$$\rho = \rho_g + (\rho_l - \rho_g)\tilde{\alpha} \quad\text{and}\quad \mu = \mu_g + (\mu_l - \mu_g)\tilde{\alpha} \tag{4}$$

where $\tilde{\alpha}$ is a smoothed field of α using a smoothing function described by Rudman [62].

The governing equations are discretized by the finite differences method. The convective terms are approximated by a third-order accurate upwind scheme, the diffusive and pressure terms by fourth-order central schemes and the time derivatives by an implicit second order backward scheme. A coupling between the pressure and the velocity is used which is based on the simultaneous update of the dependent variables. The approach is SIMPLE like and described in detail for single-phase flows by Fuchs and Zhao [12].

2.1. Turbulence modeling

The turbulent flow field is simulated by performing a LES, where the discretization scheme applied on the grid acts as a low-pass filter. A detailed discussion concerning LES can be found, for instance, in the textbooks of Pope [55] or Sagaut [63]. The grid size, h, is considerably smaller than the largest flow scales but it is larger than the Kolmogorov eddies ($l_0 \gg h \gg \eta$) for large Reynolds numbers. Therefore, the large scale structures are captured, while the small scale structures are filtered out. When applying any spatial filtering to the governing equations, new terms appear; these are called Sub-Grid-Scale (SGS) terms. LES is based on Kolmogorov's hypothesis: the large scale structures are dependent on the specific flow situation, while the behavior of the small scale structures is isotropic and geometry independent, i.e. universal. If the scales that are filtered out are small enough to be considered as universal, the SGS terms can be closed by a turbulence model.

A large number of models have been formulated in the past out of which many are based on the simple Smagorinsky model [70]. A widely used variant is the dynamic calculation of the Smagorinsky constant [15] using the least-square technique and averaging in one direction as proposed by Lilly [42]. This approach has been implemented to study a wide range of flows such as pneumatic conveying [22], reactive flows [40] or the atmospheric boundary layer [35], just to name a few.

As an indicator for the definition of an appropriate grid size the size of the Taylor scale eddies can be used, as they are defined to be located between integral scale and Kolmogorov scale eddies. In general it can be stated that the smaller the filter size is the smaller is the contribution of the SGS terms and the more accurate the solution will be. If the grid is fine enough, the contribution of SGS terms even vanishes and can therefore be neglected.

The SGS terms have a function of dissipating energy that is transferred by the energy cascade. To account for dissipation in this work the 'implicit turbulence model' [4] with no explicit SGS expression is used. By not including explicit dissipation, the overall dissipative properties of the discrete system are reduced. The neglected dissipative effects of an eventual explicit SGS model are accounted for by using dissipative numerical schemes. It must be emphasized that one may rely on such a model only if the resolution is fine enough, i.e. a considerable part of the turbulence energy spectrum is resolved.

The implicit LES approach has been successfully applied in comparable works as well, e.g. by Desjardins et al. [6]. In our simulations the grid is chosen to be approximately three times finer than the size of Taylor scale eddies. It is shown in Section 4.1 that the influence of the unresolved scales on the velocity field can be considered negligible. In fact, the limiting parameter for the grid resolution in the herein studied cases are apparently not the turbulent scales but the droplet sizes. Therefore, the preference of the simple implicit LES over a more complex model is justified.

2.2. Surface tension modeling and motion of the phase interface

Following the Continuum Surface Force (CSF) model as described in [5], the Dirac function and the interface unit normal in Eq. (2), are replaced by

$$\delta n_i = \frac{\partial \alpha}{\partial x_i}. \tag{5}$$

The normal direction of the interface, which is needed for the phase transport and the curvature, is derived from the α field using the DAN model as presented by Lörstad and Fuchs [47]. To reduce the computational effort, the calculations are carried out in the direction of the largest component of the normal vector. A distance function, Λ, is introduced which is estimated based on the volume fractions of the neighboring cells. These volume fractions are summed up in the calculation direction. It gives the distance of the interface in the neighboring cells to the center of the current cell. For the z-direction this leads to the expression for the interface normal, namely

$$n = \begin{pmatrix} n_x \\ n_y \\ n_z \end{pmatrix} = \frac{\frac{\partial \alpha}{\partial x_z}}{|\frac{\partial \alpha}{\partial x_z}|} \cdot \begin{pmatrix} -\frac{\partial \Lambda}{\partial x_x} \\ -\frac{\partial \Lambda}{\partial x_y} \\ 1 \end{pmatrix}. \tag{6}$$

This procedure, as it considers only the largest normal component, is simpler and faster as comparable methods, for example those proposed by Puckett et al. [57] or Renardy and Renardy [59].

Finally, the curvature is calculated applying the DAC model, as given by Lörstad and Fuchs [47]. As for the DAN model, the computational effort is reduced by carrying out the calculations in the direction of the largest normal component. In a similar way a distance function Λ is established. For the z-direction the expression for the interface curvature is given by

$$\kappa = \frac{n_z}{|n_z|}\left(\frac{\Lambda_{ii}}{|n|} - \frac{\Lambda_i\Lambda_j\Lambda_{ij}}{|n|^3}\right). \tag{7}$$

To apply the surface tension forces to the flow equations, the topology of the gas-liquid interface needs to be known. Therefore, for the phase field, α, which represents the liquid volume fraction, the transport equation

$$\frac{\partial \alpha}{\partial t} + \frac{\partial u_i \alpha}{\partial x_i} = 0 \qquad (8)$$

is solved. When solving this equation it is of utmost importance to be not too diffusive in order to keep the liquid gas interface sharp and to use a stable approach at the same time.

Several approaches have been proposed and compared by Rudman [61] and Gopala and van Wachem [17]. In both papers the ability to keep the interface sharp and the mass conserved has been studied with simplified advection and shear flow cases and a case capturing the progression of the Rayleigh–Taylor instability. Rudman [61] reported the superior behavior of the direction split method proposed by Young [79] compared to the Simplified Line Interface Calculation (SLIC) method [52], the original VOF method [30] and the flux-corrected transport (FCT) method proposed by Rudman [61]. Gopala and van Wachem [17] considered the Lagrangian Piecewise Linear Interface Construction (PLIC) [75], the CICSAM [73] and the inter-gamma differencing scheme [31] to be preferable over the above mentioned FCT method.

Based on the discussion above, the direction split method proposed by Young [79], extended from 2D to 3D is applied in this work. For details concerning the implementation, the reader is referred to the original paper by Lörstad [44].

Lörstad et al. [45,46], Lörstad and Fuchs [47] and Lörstad [44] reported several test cases which prove the quality of the above described VOF methodology. A three-dimensional Stokes flow (Re = 10⁻⁶) past a fix liquid sphere represents one of them. The simulations for different viscosity ratios were compared to analytical solutions given by Panton [54]. For a viscosity ratio of unity the results indicated that the flow solution is second order accurate [47]. However, the viscosity model (c.f. Eq. (4)) seems to introduce a first order error. The same conclusions were drawn when the velocity of a bubble rising in a quiescent liquid due to gravity was computed on different grid resolutions.

Furthermore, three-dimensional advection tests similar to the one used by Aniszewski et al. [1] and the two-dimensional tests by Rudman [62] and Gerlach et al. [14] were performed [47]. Herein, a liquid of an initially spherical shape is deformed by a pre-defined flow field. After a certain period of time the flow is reversed which would result, in the case of a perfect advection scheme, in a liquid of the initial shape. This type of tests evaluate the phase transport model and the DAN model. Second order accuracy was found for unidirectional and rotating flow fields while the accuracy showed to reduce slightly for large deformations.

The results of a commonly used case [e.g. by [1,14,37,49,56,59,77]] to test the surface tension modeling are given by Lörstad et al. [45,46]. Therein, a droplet is placed in a zero velocity field as initial and boundary condition. The solution is usually subjected to spurious unphysical currents. The order of accuracy showed to be the same than for the immersed boundary method and the PROST VOF-model by Renardy and Renardy [59] even though the magnitude of the error is slightly larger. However, the spurious currents diminished with time. Moreover, the test revealed that, if the droplet is resolved by ten cells over the diameter, the maximum error for κ is approximately 4%. As the Weber numbers in engines are usually large, the error originating from the surface tension term is considered to be small.

Additionally to the above discussed tests, the VOF/DAC/DAN approach has been successfully compared to experimental results for air bubbles rising in water due to gravity (by Lörstad and Fuchs [47] for a similar set-up than the one used by Popinet [56]) and air injection into a water channel [44].

3. Description of the ODT model

For comparison of the droplet size distributions obtained by the VOF approach, in the present study the ODT model is applied. The model is summarized in the following section. However, for a detailed description of the method, the reader is referred to its original formulation by Kerstein [33] and its extensions by Kerstein et al. [34] and Ashurst and Kerstein [2].

ODT is a stochastic model resolving a turbulent flow along a notional line of sight through a 3-dimensional flow. The main advantages of such a one-dimensional stochastic simulation approach are twofold. First, a one-dimensional formulation enables affordable simulations of high Reynolds number turbulence over the full range of relevant length and time scales. On the contrary, computational cost considerations often limit the application of DNS to flows of moderate Reynolds numbers. Second, the model has proven to successfully capture diverse flow behaviors. Furthermore, it permits high resolution of property gradients, which is needed to capture details of, e.g., boundary layers, flame structures and flow structures close to phase boundaries.

ODT has recently been used by Movaghar et al. [51] to model the primary breakup of statistically stationary turbulent liquid jets. This was achieved by extending ODT to deal with the interaction between turbulence and surface tension energy. Moreover, Rayleigh type wave instabilities and shear driven breakup mechanism were accounted for.

The flow on an ODT line is time-advanced by solving a set of equations given by

$$\frac{Du_i(y,t)}{Dt} = \nu \frac{\partial^2 u_i(y,t)}{\partial y^2} - S_{u_i} \qquad (9)$$

$$\frac{D\phi(y,t)}{Dt} = \varrho \frac{\partial^2 \phi(y,t)}{\partial y^2} - S_\phi . \qquad (10)$$

Here, u_i are the velocity components and ϕ is a passive scalar. The coefficients ν and ϱ denote the molecular viscosity and mass diffusivity, respectively. S_{u_i} and S_ϕ represent source terms. In the present application the turbulent jet decays and S_{u_i} is equal to zero.

In ODT turbulent advection is modeled by a series of stochastic eddy events. Each eddy event is modeled by applying an instantaneous mapping of the property field, called triplet map [c.f. [51]]. ODT samples eddy events from an instantaneous eddy event rate distribution that evolves with the flow. These events are individually parameterized by the position y_0 and the size l. The reconstruction of the distribution every time an eddy event or an advancement of Eq. (9) takes place is computationally expensive. Therefore, for computational efficiency in ODT eddy events are sampled using an equivalent Monte-Carlo numerical procedure called thinning which was originally proposed by Lewis and Shedler [41]

4. Results and discussion

The VOF simulations presented herein were run in simple cuboid domains as sketched in Fig. 1. A Dirichlet condition was applied at the inlet, i.e. the velocity vector is given. The velocity components and scalars at the outlet correspond to a zero-gradient condition. At the walls no-slip and zero-gradient was imposed for the velocity components and the scalars, respectively.

The computed operation conditions are oriented on realistic parameters of Diesel injection. However, to improve numerical stability, the liquid-gas viscosity and density ratio were reduced. The inlet nozzle was assumed to have a diameter of $d_{noz} = 10^{-4}$ m. A uniform velocity profile at the nozzle orifice of $U_{inj} = 500$ m/s was
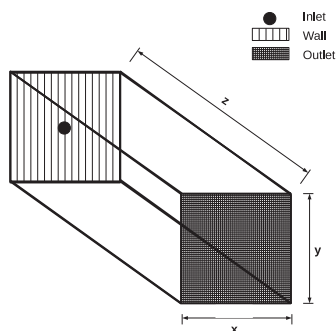
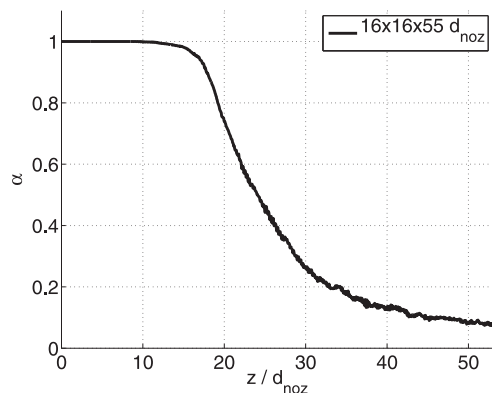**Fig. 1.** Geometry of the domain used in the VOF simulations and boundary conditions.

Fig. 2. Average liquid volume fraction along the jet centerline. The jet is considered to be atomized at a downstream position of $z = 30 \, d_{\text{noz}}$. The parameters of the jet are $Re_{\text{jet}} = 15{,}000$, $We_{\text{jet}} = 10{,}000$, $\rho_l/\rho_g = 10$ and $\mu_l/\mu_g = 3.42$.
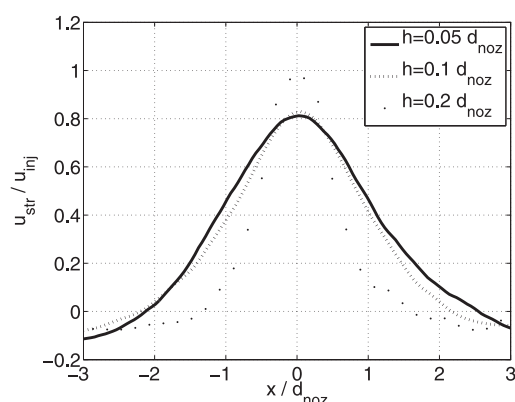

Fig. 3. Average streamwise velocity at a downstream position of $z = 30 \, d_{\text{noz}}$ for different grid resolutions. The simulations performed with a grid resolution of $h = 0.05 \, d_{\text{noz}}$ are considered to give grid independent results for the velocity. The parameters of the jet are $Re_{\text{jet}} = 15{,}000$, $We_{\text{jet}} = 10{,}000$, $\rho_l/\rho_g = 10$ and $\mu_l/\mu_g = 3.42$.

considered. All results presented within this paper are normalized to d_{noz} and U_{inj}.

In the following section the sensitivity of results obtained by VOF to numerical parameters, namely the grid resolution and domain size, is assessed. Afterwards the effect of varying the liquid-gas density and viscosity ratio is evaluated. Further, the results are compared to data obtained using the ODT method. Finally, the influence of in-nozzle flow on the jet development is studied.

4.1. Sensitivity of VOF to numerical parameters

The objective of the present study is to study the primary break-up of a liquid jet. For this purpose, a plane normal to the z-axis was introduced in the domain where the liquid phase which passes by is analyzed. The algorithm to extract information concerning the liquid is based on the algorithm described by Herbert et al. [28] and extended by Grosshans et al. [23–25] to time dependent problems. By identifying the connected liquid phase which passes the layer per timestep, the total volume of each liquid structure is determined. This quantity is used to calculate the radius equivalent to a spherical droplet.

To capture the characteristics of the fully atomized jet, this plane needs to be placed far enough downstream of the injector. On the other hand, it shall be close enough to the nozzle so the droplets are large enough to be accurately described by the VOF approach.

To define the appropriate position for this plane, a jet of $Re_{\text{jet}} = 15{,}000$ and $We_{\text{jet}} = 10{,}000$ was simulated. Moreover, a liquid-gas density and viscosity ratio of 10 and 3.42, respectively, were maintained. For this configuration the speed of sound is estimated to be 1500 m/s inside the liquid and 660 m/s inside the gas. Thus, the flow can be considered incompressible within the largest part of the domain. The dimensions of the computational domain were $x \times y \times z = 16 \times 16 \times 55 \, d_{\text{noz}}$ containing cells of a uniform size of $h = 0.05 \, d_{\text{noz}}$. It is shown below that this numerical set-up is well chosen.

The resulting average liquid volume fraction along the jet centerline, see Fig. 2, is chosen as the criterion to identify the position of the jet break-up. For regions of the intact liquid jet a liquid volume fraction of unity is observed. Thus, the jet starts to break up after a downstream position of $z = 13 \, d_{\text{noz}}$. It is decided to consider the jet to be fully broken up when the centerline liquid volume fraction is below 0.25. Thus, in the following the characteristics of the atomization is assessed at a downstream position of $z = 30 \, d_{\text{noz}}$.

To test the grid sensitivity of the results, the VOF equations were solved on different resolutions including cell sizes of 0.2, 0.1 and 0.05 d_{noz}. The resulting average streamwise velocity profiles at a downstream position of $z = 30 \, d_{\text{noz}}$ are shown in Fig. 3. The

coarsest grid in the case of $h = 0.2 \, d_{\text{noz}}$ causes high numerical diffusion which damps turbulence. Thus, the spray does not widen up as much as it can be seen for finer grids. The velocity profiles relating to grid resolutions of $h = 0.1 \, d_{\text{noz}}$ and $h = 0.05 \, d_{\text{noz}}$ are very similar. Comparing their centerline velocity a difference of less than 4% is observed. Therefore, the simulations performed with a grid resolution of $h = 0.05 \, d_{\text{noz}}$ are considered to give grid independent results for the velocity.

This is supported by a Richardson extrapolation [according to the procedure described by Roache [60]] concerning the same simulations which has been reported by Grosshans [19] and Grosshans et al. [26]. They evaluated the average streamwise velocity for three points in the domain. In summary, the apparent order of discretization showed to be between 2.5 and 3.7, which is in the expected range. The relative errors for $h = 0.05 \, d_{\text{noz}}$ were considered to be sufficiently low.

Besides the velocities, also the grid sensitivity of the resulting drop size distributions was analyzed. The high sensitivity of the droplet diameters to the used grid resolution has been pointed out earlier, e.g. by Gorokhovski and Herrmann [18]. Results extracted at $z = 30 \, d_{\text{noz}}$ are presented in Fig. 4. Further to the above reported grid resolutions, an even finer grid, namely $h = 0.0375 \, d_{\text{noz}}$, was included in the study. It is interesting to note that the droplet diameter distributions obtained with a cell size of $h = 0.05 \, d_{\text{noz}}$ are relatively reliable down to a droplet diameter of $d_d/h = 2$. This confirms the excellent ability of the DAC/DAN method to capture the curvature of the liquid-gas interface. Nevertheless, smaller
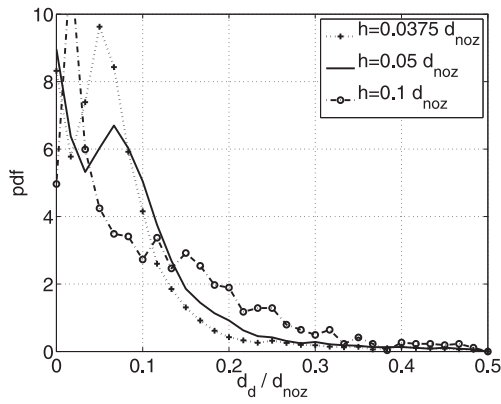
Fig. 4. Droplet diameter distributions at a downstream position of $z = 30\ d_{\mathrm{noz}}$ for different grid resolutions. The results confirm the ability of the DAC/DAN approach to capture the curvature of the liquid-gas interface down to droplet sizes of $d_d/h = 2$. Smaller droplets are, however, not resolved. The parameters of the jet are $Re_{\mathrm{jet}} = 15,000$, $We_{\mathrm{jet}} = 10,000$, $\rho_l/\rho_g = 10$ and $\mu_l/\mu_g = 3.42$.
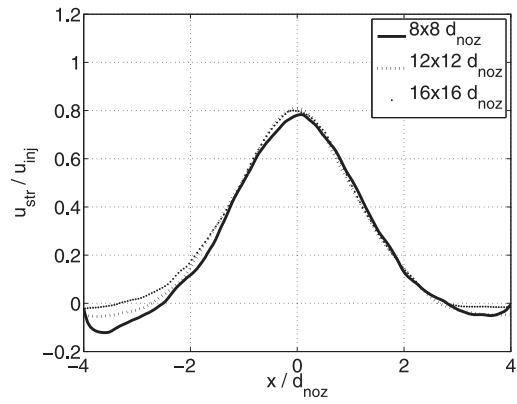
Fig. 5. Average streamwise velocity at a downstream position of $z = 30\ d_{\mathrm{noz}}$ for different domain sizes. The velocity profiles in spanwise direction of $\pm 2\ d_{\mathrm{noz}}$ are nearly identical. Thus, a domain of the size of 8 d_{noz} in x and y-direction is judged to be sufficient. The parameters of the jet are $Re_{\mathrm{jet}} = 15,000$, $We_{\mathrm{jet}} = 10,000$, $\rho_l/\rho_g = 10$ and $\mu_l/\mu_g = 3.42$.

droplets are not properly resolved. However, the droplets which are smaller than $d_d/h = 2$ contribute only 0.87% to the total liquid mass at the considered downstream position. The low liquid mass carried by the unresolved droplets carries, due to their small size, little kinetic energy. Thus, the related error is small.

On the other hand all investigated cases are of a high Weber number. Therefore, the surface tension term, and consequently the interface curvature has a low contribution to the momentum equation, c.f. Eq. (2). This explains why the velocity profiles presented in Fig. 3 show a better convergence than the corresponding droplet diameter distributions.

Following the above discussions, the simulations described in the following were run on a grid with a cell size of $h = 0.05\ d_{\mathrm{noz}}$.

Not only the grid resolution but also the domain size is investigated. Therefore, the above described jet was run is run in a domain of the size of 8, 12 and 16 d_{noz} in x and y-direction. The average streamwise velocity profiles at a downstream position of $z = 30\ d_{\mathrm{noz}}$ are shown in Fig. 5. It can be seen that the velocities at the centerline and in an area in spanwise direction of $\pm\ 2\ d_{\mathrm{noz}}$ are nearly identical. This is the region where by far most of the liquid mass is transported. Thus, a domain of the size of 8 d_{noz} in x and y-direction is judged to be sufficient and was considered in the following simulations.

4.2. Liquid-gas density ratio and comparison to ODT

To assess the sensitivity of the atomization on the fluid properties, simulations with liquid-gas density ratios of 10, 20 and 30 were performed. The other conditions are identical to those described in the previous section, namely $Re_{\mathrm{jet}} = 15,000$, $We_{\mathrm{jet}} = 10,000$ and $\mu_l/\mu_g = 3.42$.

Snapshots of the penetration of the liquid jet of a liquid-gas density ratio of 10 are shown in Fig. 6. Fig. 6(b) depicts the jet very short after the beginning of the injection forming a mushroom cap shape. In Fig. 6(c) a detail of the liquid core at later stage is enlarged. One can see the formation of Kelvin–Helmholtz instabilities at the surface. These lead to the stripping off of small droplets from the jet surface. As these droplets are small, their Stokes number is also small, hence their trajectories are strongly influenced by turbulent eddies, which leads to the dispersion of the spray.

The droplet diameter distributions for different liquid-gas density ratios are presented in Fig. 7. The results of the VOF simulations (Fig. 7(a)) are compared to the results of the ODT simulations (Fig. 7(b)).

In opposite to the ODT simulations, the VOF distributions stemming from the simulations show two peaks. The first peak is located around $d_d/d_{\mathrm{noz}} \approx 0.02$ and the second peak around $d_d/d_{\mathrm{noz}} \approx 0.08$. While the second peak is close to the resolution limit of the method, the first peak is clearly beneath. In the resolved region, both simulation types give distributions of a similar shape. However, the droplets predicted by ODT are generally larger that those resulting from the VOF simulations. This is also related to the method to analyze the droplets: the sizes predicted by ODT relate to droplets which are generated directly by the primary break-up. Thus, they did not experience any secondary break-ups which further decrease the droplet size. The droplets presented in Fig. 7(b) are, therefore, not related to a fixed position in space. Instead the distribution includes all droplets which are separated at any time from the liquid core. The VOF results (Fig. 7(a)), on the other hand, represent droplet distributions obtained at a fixed plane in space. Therefore, also a certain amount of secondary breakups is included in the results. Consequently, the distributions predicted by VOF show smaller droplets compared to ODT.

While the limitation of the VOF results correspond to the applied grid resolution, the leading order error in the ODT is assumed to be related to not capturing 3-dimensional effects. Thus, the effect of swirls or vortices are not reflected in the results presented in Fig. 7(b).

Comparing the simulations of different liquid-gas density ratios with each other, both VOF and ODT show little differences. Thus, both approaches indicate a low sensitivity of the droplet size distributions to the range of studied conditions. However, the VOF approach predicts more large, i.e. resolved, droplets the higher the liquid-gas density ratio is. For lower liquid-gas density ratios the jet breaks up faster, generating smaller droplets through secondary breakup.

The streamwise and spanwise droplet velocities of the three cases predicted by VOF are presented in Fig. 8. The case of the highest density ratio shows the fastest and the case of the lowest density ratio the slowest droplets, c.f. Fig. 8(a). This is reasonable since larger droplets have a higher inertia and therefore their trajectories are the least disturbed by turbulent eddies. In the case of the low density ratio, the droplets are the smallest and the aerodynamic drag force acting on the droplets is the highest due to a high gas density. However, the spanwise droplet velocity distribution (Fig. 8(b)) is only little influenced in the range of studied conditions.
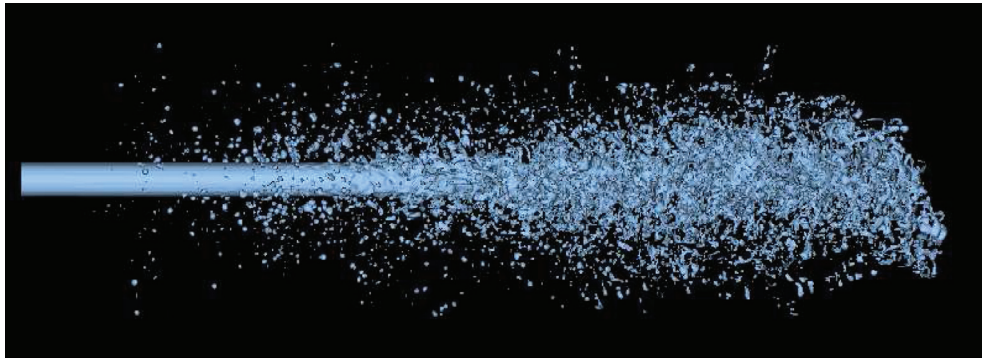
(a) The complete jet at $t = 42.6$. The blue surface describes the isosurface of $\alpha = 0.5$.
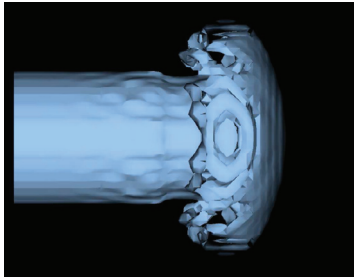
(b) The jet at $t = 1.1$, forming a mushroom cap shape.
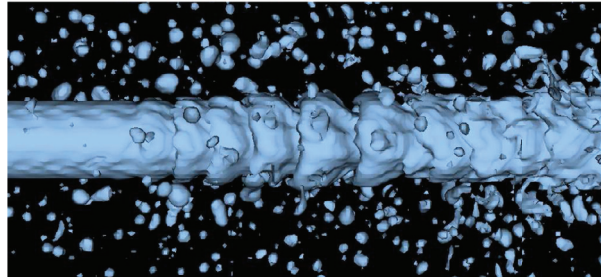
(c) Detail of the jet between $z = 8$ and $z = 16$ at $t = 58.6$, forming Kelvin-Helmholtz instabilities on the liquid surface.

Fig. 6. Snapshots of the jet penetration of case of $Re_{jet} = 15{,}000$, $We_{jet} = 10{,}000$, $\rho_l/\rho_g = 10$ and $\mu_l/\mu_g = 3.42$. (For interpretation of the references to colour in this figure legend, the reader is referred to the web version of this article.)
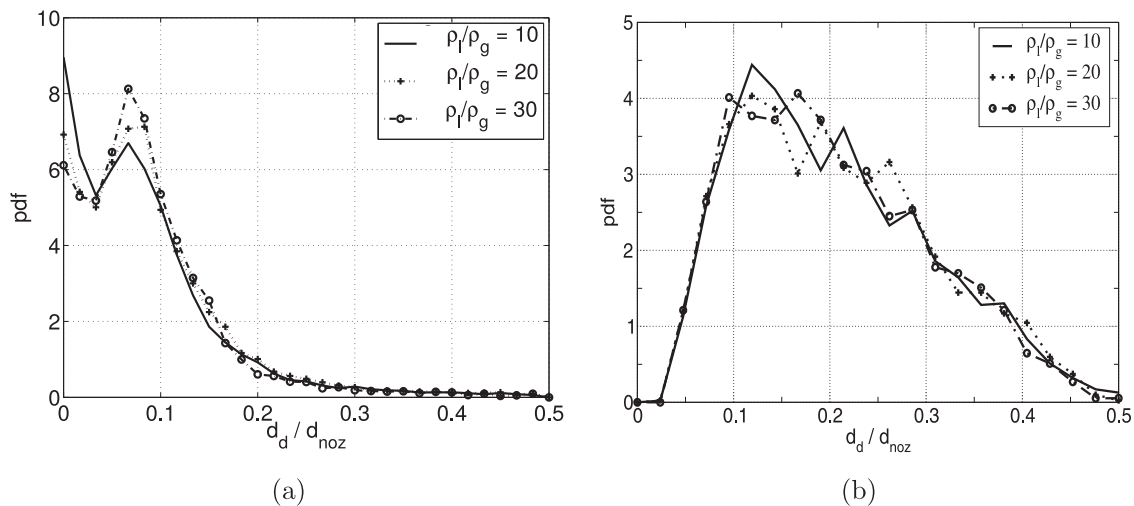
Fig. 7. Droplet diameter distributions at a downstream position of $z = 30\, d_{noz}$ resulting from the VOF (a) and the ODT (b) simulations for variations of the liquid gas density ratio. The parameters of the jet are $Re_{jet} = 15{,}000$, $We_{jet} = 10{,}000$ and $\mu_l/\mu_g = 3.42$.

4.3. Liquid-gas viscosity ratio

Further, the influence of the liquid-gas viscosity ratio on the primary break-up was computed using VOF. For this purpose liquid jets of the properties $\mu_l/\mu_g = 1$, 2 and 7 were simulated. The other conditions are identical to those described in the previous section, namely $Re_{jet} = 15{,}000$ and $We_{jet} = 10{,}000$ while ρ_l/ρ_g was set to 10.

The resulting droplet diameter distributions are presented in Fig. 9. In opposite to the results for different density ratios, the distributions for different viscosity ratios differ significantly from each other. The case of the smallest liquid-gas viscosity ratio creates the largest droplets, while the case of the highest liquid-gas viscosity ratio creates the smallest droplets. As the jet Reynolds number is kept constant for the three cases, an increase in the liquid-gas viscosity ratio results in an increase of the Reynolds
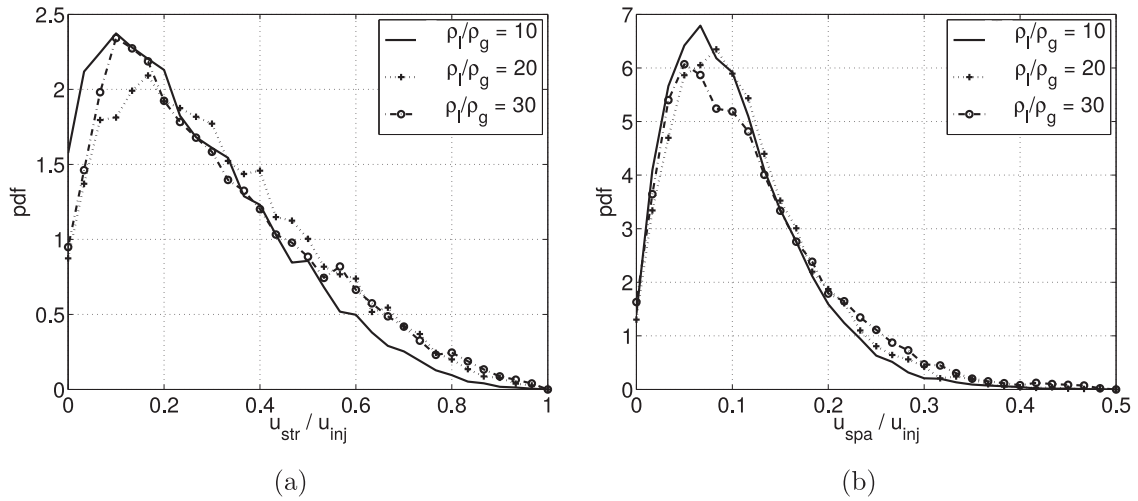
Fig. 8. Streamwise (a) and spanwise (b) droplet velocity distributions at a downstream position of $z = 30\ d_{noz}$ resulting from the VOF simulations for variations of the liquid gas density ratio. The parameters of the jet are $Re_{jet} = 15{,}000$, $We_{jet} = 10{,}000$ and $\mu_l/\mu_g = 3.42$.
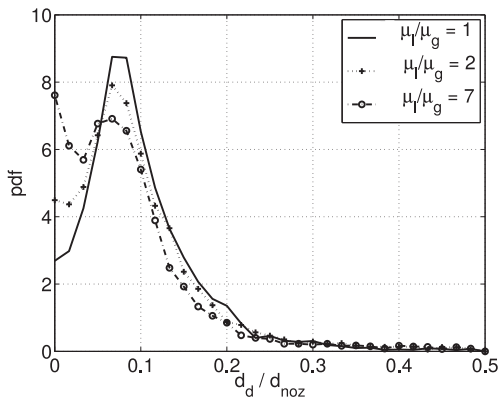

Fig. 9. Droplet diameter distributions at a downstream position of $z = 30\ d_{noz}$ resulting from the VOF simulations for variations of the liquid gas viscosity ratio. The parameters of the jet are $Re_{jet} = 15{,}000$, $We_{jet} = 10{,}000$ and $\rho_l/\rho_g = 10$.
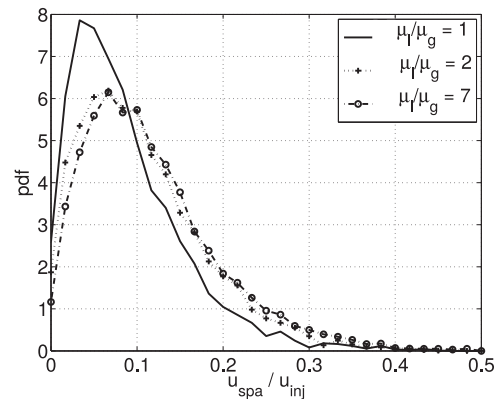

Fig. 10. Spanwise droplet velocity distributions at a downstream position of $z = 30\ d_{noz}$ resulting from the VOF simulations for variations of the liquid gas viscosity ratio. The parameters of the jet are $Re_{jet} = 15{,}000$, $We_{jet} = 10{,}000$ and $\rho_l/\rho_g = 10$.

number of the gaseous phase. This leads to more turbulent structures in the gas, which enhance the instability mechanisms acting on the liquid surface. These instabilities cause breakups and, consequently, smaller droplets.

Since small droplets have less inertia than large droplets, thus, their trajectories are more influenced by turbulent eddies. Furthermore, in cases of a viscosity ratio of 2 and 7, for which the smallest droplets occur, the gaseous phase contains the most turbulent structures. For this reason the droplets are the most dispersed in these cases and their spanwise velocities, (c.f. Fig. 10) are the highest.

The average streamwise velocity profiles as function of variations of the liquid-gas viscosity ratio are depicted in Fig. 11. The negative streamwise velocities in this region account for the backflow which is caused by the air entrained by the spray. The cases containing the largest droplets, i.e. for a low viscosity ratio, show the highest centerline velocity, due to the high inertia of the droplets. The smaller the droplets, the lower the centerline velocity and the more the spray is widened up due to turbulent dispersion.

4.4. In-nozzle flow

The cases considered so far employ a uniform velocity profile as inlet condition for the liquid jet. To assess the jet development
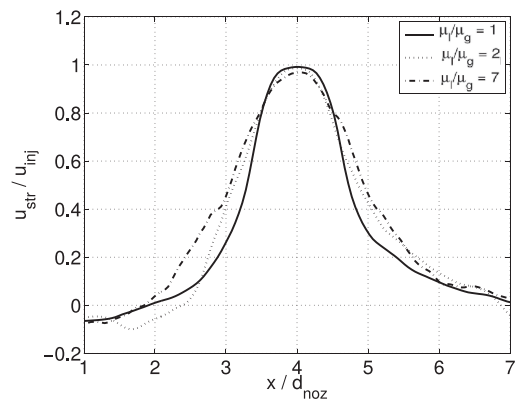

Fig. 11. Average streamwise velocity at a downstream position of $z = 30\ d_{noz}$ for different liquid gas viscosity ratio resulting from the VOF simulations. The parameters of the jet are $Re_{jet} = 15{,}000$, $We_{jet} = 10{,}000$ and $\rho_l/\rho_g = 10$.

under conditions closer to real fuel injection, the influence of the flow inside the nozzle is taken into account.

In a separate simulation the flow inside a nozzle was computed and provided by Altimira (2013)[1] using the OpenFOAM solver

---

[1] Personnal communication.

in-nozzle

in-nozzle, hot fuel

$t = 71$
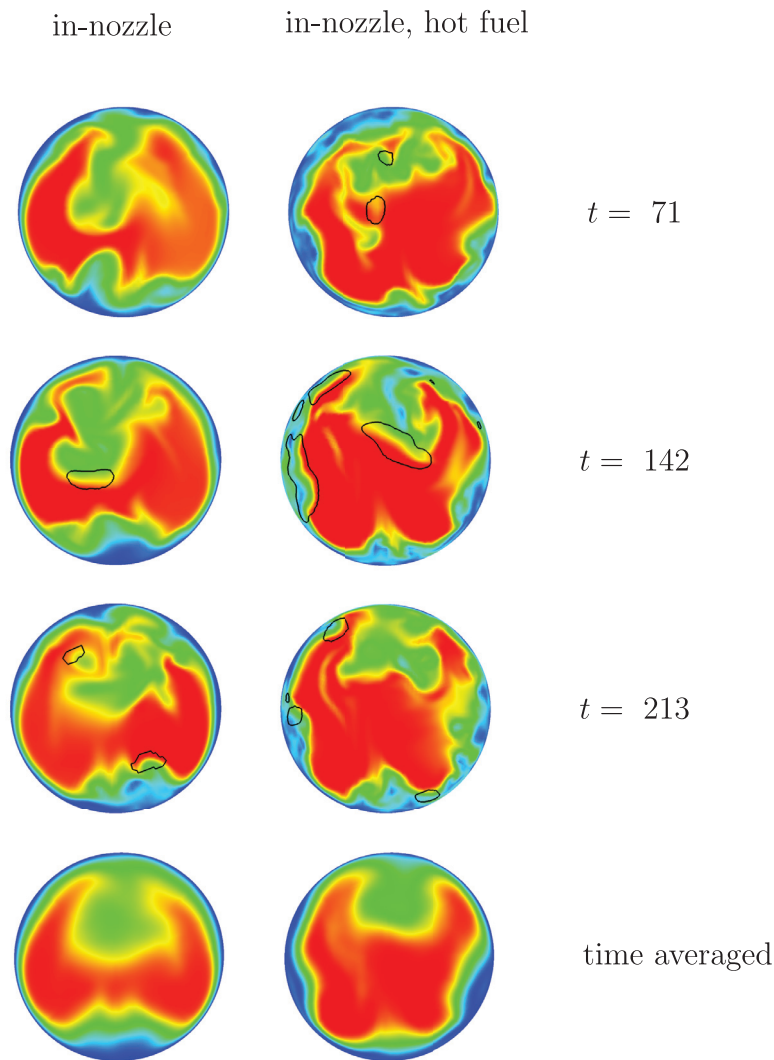
$t = 142$

$t = 213$

time averaged

Fig. 12. Instantaneous and time averaged fields at the nozzle orifice plane which are used as starting condition of the jet to simulate the effect of the in-nozzle flow (left) and the in-nozzle flow of hot fuel (right). The color gives the velocity magnitude where the blue color corresponds to zero and the red color to the maximum velocity. The black lines indicate the location of cavitation bubbles. (For interpretation of the references to colour in this figure legend, the reader is referred to the web version of this article.)

interPhaseChangeFoam. The chosen geometry corresponds to a representative Diesel nozzle of an orifice diameter of 130 μm.

The in-nozzle simulation applied a LES-VOF approach taking into account the generation of cavitation bubbles. Two different inlet flow fields were considered which both reflect the turbulence and cavitation inside the nozzle. However, while the liquid in one simulation is at ambient temperature (298 K), the second simulation accounts a liquid temperature of 348 K. The results of these simulations in terms of velocity profiles and liquid volume fractions served as instantaneous inlet conditions for the jet simulations presented herein. Instantaneous snapshots and time averages of the inlet conditions at the orifice plane are given in Fig. 12. For both cases the asymmetry of the profiles caused by the in-nozzle geometry can be observed. For comparison, a third case is run applying a uniform velocity profile at the inlet.

All three cases have a jet Reynolds number of 8000 and a jet Weber number of 330. The density ratio of the liquid and the cavitation vapor bubbles was 480 in the in-nozzle simulations. The corresponding ratio of viscosity was 88. Due to numerical stability issues, the liquid-gas density and viscosity ratios are reduced to 18 in the liquid jet simulation. For simplification, the vapor bubbles, originated from cavitation in the nozzle, are assumed to be of the same properties as the surrounding gas phase. It is recalled from Section 2 that no phase change model is applied.

With the discussion in the introduction in mind, it is expected that the in-nozzle flow will create disturbances transported through the liquid jet and leading to a faster break-up. This is confirmed when looking at the snapshots of the jet development in Fig. 13. While the jet started with a top-hat profile propagates straight, the jets of the cases accounting for in-nozzle turbulence are stronger disturbed and propagate slower. As the collapse of cavitation bubbles is not modeled here, this effect is caused by turbulent structures created inside the nozzle. Also, the gas bubbles inside the liquid jet caused by cavitation in the nozzle enhance the break-up. The propagation of the tip of the liquid jets over time is shown in Fig. 14. The figure confirms that the undisturbed jet propagates faster, while the effect of the increased liquid temperature is small.

Further, the influence of the in-nozzle flow on the liquid gas mixing is evaluated. The instantaneous mixing is quantified based on a mixing indicator proposed by Grosshans [19], Grosshans et al. [26]. This indicator is based on the rms of the liquid volume fraction in the complete domain, rms(α). rms(α) is normalized to the theoretical value of the rms of the liquid volume fraction,
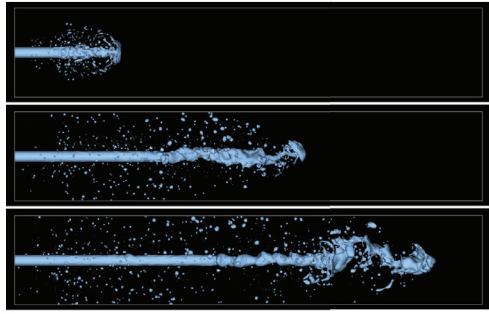
(a)
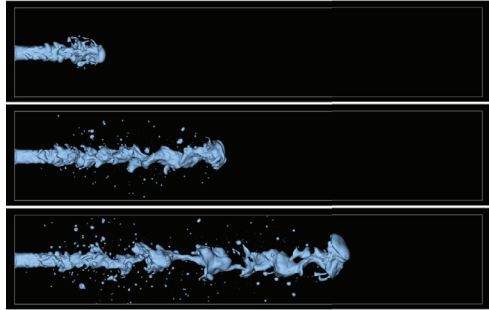
(b)
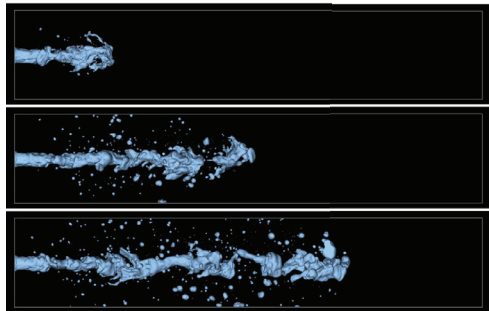
(c)

Fig. 13. Liquid jet evolution, started with a top hat profile (a), accounting for in-nozzle turbulence, (b) and accounting for in-nozzle turbulence plus increased liquid temperature (c). Each case is shown for $t = $ 11.5, 32.6 and 55.7. The parameters of the jets are $Re_{jet} = 8000$, $We_{jet} = 330$, $\rho_l/\rho_g = 18$ and $\mu_l/\mu_g = 18$.
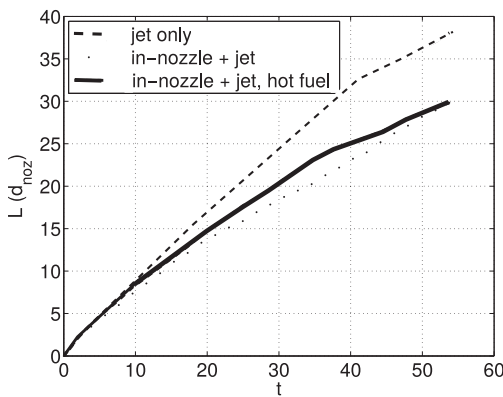

Fig. 14. Liquid penetration over time in non-dimensional units. The undisturbed jet propagates faster, while the effect of the increased liquid temperature is small. The parameters of the jets are $Re_{jet} = 8000$, $We_{jet} = 330$, $\rho_l/\rho_g = 18$ and $\mu_l/\mu_g = 18$.
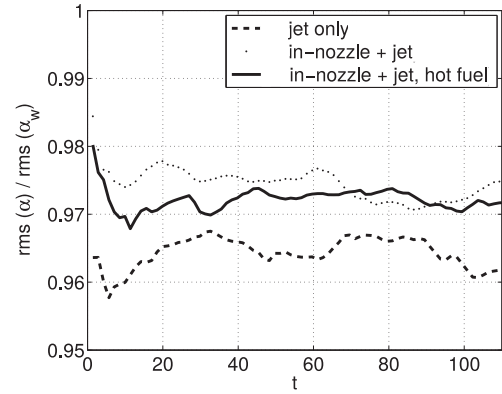

Fig. 15. Time evolution of the liquid-gas mixing. The relative velocity at the liquid-gas interface after the injection is reduced for the cases considering the in-nozzle flow. Thus, less small droplets are sheared of and the liquid-gas mixing reduces in comparison to the case employing a top hat profile at the inlet. The parameters of the jets are $Re_{jet} = 8000$, $We_{jet} = 330$, $\rho_l/\rho_g = 18$ and $\mu_l/\mu_g = 18$.

relating to the liquid which is currently in the domain, if no mixing would occur at all, denoted as rms(α_w). Thus, the mixing indicator is always between unity and zero, whereas a decrease in the mixing indicator corresponds to a better liquid-gas mixing in the domain. The time evolution of this indicator is shown in Fig. 15 for the three simulated cases. The curves reveal that when employing a top-hat profile, the mixing is significantly better compared to the other two cases. This is due to the higher relative velocity at the liquid-gas interface after the injection. Consequently, small droplets are sheared off at the liquid surface. These small droplets can also be observed when comparing the snapshots of the three cases in Fig. 13.

5. Conclusions

The outcome of liquid injection into a stagnant gas has been evaluated depending on the physical and numerical parameters. It has been demonstrated in this paper that the VOF/DAC/DAN method represents an accurate and efficient alternative to simulate the primary breakup of a liquid jet. For comparison, three cases of different liquid-gas density ratios have been calculated using the ODT model. Both methods predict similar features of the droplet size distributions, indicating that the disintegration of the liquid core into ligaments and droplets due to aerodynamic instabilities has been captured. However, the comparison also showed the limitation of the VOF approach to resolve small droplets depending on the grid resolution.

The influence of varying the liquid-gas density ratio between 10 and 30 on the aerodynamic break-up was demonstrated to be low. On the other hand, the reduction of the liquid-gas viscosity ratio from 7 to 1 resulted in smaller droplets and consequently a stronger dispersion. This is attributed to the increased turbulence in the gas phase, enhancing instabilities at the liquid-gas interface. Furthermore, in-nozzle turbulence and cavitation bubbles was shown to quicken the liquid core break-up.

References

[1] Aniszewski W, Ménard T, Marek M. Volume of fluid (VOF) type advection methods in two-phase flow: A comparative study. Comput Fluids 2014;97:52–73.

[2] Ashurst W, Kerstein A. One-dimensional turbulence: Variable-density formulation and application to mixing layers. Phys Fluids 2005;17.

[3] Berrocal E, Kristensson E, Richter M. Application of structured illumination for multiple scattering suppression in planar laser imaging of dense sprays. Opt Express 2008;16:17870–81.

[4] Boris J, Grinstein F, Oran E, Kolbe R. New insights into large eddy simulation. Fluid Dyn Res 1992;100:199–228.

[5] Brackbill J, Kothe D, Zemach C. A continuum method for modeling surface tension. J Comput Phys 1992;100:335–54.

[6] Desjardins O, Moureau V, Pitsch H. An accurate conservative level set/ghost fluid method for simulating turbulent atomization. J Comput Phys 2008;227:8395–416.

[7] Desjardins O, Pitsch H. Detailed numerical investigations of the turbulent atomization of liquid jets. Atomiz Sprays 2010;20:311–36.

[8] Eggers J, Emmanuel V. Review of theory of distortion and disintegration of liquid streams. Rep Prog Phys 2008;71:1–79.

[9] Elkotb M. Fuel atomization for spray modelling. Prog Energy Combust Sci 1982;8:61–91.

[10] Faeth G, Hsiang L-P, Wu P. Structure and breakup properties of sprays. Int J Multiphase Flow 1995;21:99–127.

[11] Farth A, Fettes C, Leipertz A. Investigation of the diesel spray break-up close to the nozzle at different injection conditions. The fourth international symposium COMODIA 98; 1998.

[12] Fuchs L, Zhao H-S. Solution of three-dimensional viscous incompressible flows by a multi-grid method. Int J Num Meth Fluids 1984;4:539–55.

[13] Fuster D, Bague A, Boeck T, Le Moyne L, Leboissetier A, Popinet S, et al. Simulation of primary atomization with an octree adaptive mesh refinement and VOF method. Int J Multiphase Flow 2009;35:550–65.

[14] Gerlach D, Tomar G, Biswas G, Durst F. Comparison of volume-of-fluid methods for surface tension-dominant two-phase flows. Int J Heat Mass Transfer 2006;49:740–54.

[15] Germano M, Piomelli U, Moin P, Cabot W. A dynamic subgridscale eddy viscosity model. Phys Fluids 1991;1760–5.

[16] Ghiji M, Goldsworthy L, Brandner P, Garaniya V, Hield P. Numerical and experimental investigation of early stage diesel sprays. Fuel 2016;175:274–86.

[17] Gopala V, van Wachem B. Volume of fluid methods for immiscible-fluid and free surface flows. Chem Eng J 2008;141:204–21.

[18] Gorokhovski M, Herrmann M. Modeling primary atomization. Annu Rev Fluid Mech 2008;40:343–66.

[19] Grosshans H. Large eddy simulation of atomizing sprays. Lund University; 2013. Ph.d. thesis.

[20] Grosshans H, Berrocal E, Kristensson E, Szász R-Z, Fuchs L. Correlating results from numerical simulation to SLIPI-based measurements for a non-combusting diesel spray. 12th triennial international conference on liquid atomization and spray systems (ICLASS), 2–6 September 2012, Heidelberg, Germany; 2012.

[21] Grosshans H, Kristensson E, Szász R-Z, Berrocal E. Prediction and measurement of the local extinction coefficient in sprays for 3d simulation/experiment data comparison. Int J Multiphase Flow 2015;72:218–32.

[22] Grosshans H, Papalexandris M. Evaluation of the parameters influencing electrostatic charging of powder in a pipe flow. J Loss Prev Process Ind 2016;43:83–91.

[23] Grosshans H, Szász R-Z, Fuchs L. Development of a combined VOF-LPT method to simulate two-phase flows in various regimes. 7th international symposium on turbulence and shear flow phenomena, July 28–31, 2011, Ottawa, Canada; 2011.

[24] Grosshans H, Szász R-Z, Fuchs L. Full spray simulation-coupled volume of fluid and lagrangian particle tracking methods. 24th european conference liquid atomization and spray system, September 5–7, 2011, Estoril, Portugal; 2011.

[25] Grosshans H, Szász R-Z, Fuchs L. Development of an efficient statistical volumes of fluid–lagrangian particle tracking coupling method. Int J Num Meth Fluids 2014;74(12):898–918.

[26] Grosshans H, Szász R-Z, Fuchs L. Enhanced liquid–gas mixing due to pulsating injection. Comput Fluids 2015;107:196–204.

[27] Harlow F, Welch J. Numerical calculation of time-dependent viscous incompressible flow of fluid with free surface. Phys Fluids 1965;8(12):2182–9.

[28] Herbert D, Schmidt D, Knaus D, Philips S, Magari P. Parallel VOF spray droplet identification in an unstructured grid. ILASS Americas, Orlando, Florida, May 2008; 2008.

[29] Hiroyasu H, Kadota T. Fuel droplet size distribution in diesel combustion chamber. SAE 1974. 740725

[30] Hirt C, Nichols B. Volume of fluid (VOF) method for the dynamics of free boundaries. J Comput Phys 1981;39:201–25.

[31] Jasak H., Weller H.. Interface-tracking capabilities of the intergamma differencing scheme. 1995. Technical Report.

[32] Jiang X, Siamas G, Jagus K, Karayiannis T. Physical modelling and advanced simulations of gas-liquid two-phase jet flows in atomization and sprays. Prog Energy Combust Sci 2010;36:131–67.

[33] Kerstein A. One-dimensional turbulence: Model formulation and application to homogeneous turbulence, shear flows, and buoyant stratified flows. J Fluid Mech 1999;392:277–334.

[34] Kerstein A, Ashurst W, Wunsch S, Nilsen V. One-dimensional turbulence: Vector formulation and application to free shear flow. J Fluid Mech 2001;447:85–109.

[35] Kirkpatrick M, Ackerman A, Stevens DE, Mansour N. On the application of the dynamic smagorinsky model to large-eddy simulations of the cloud-topped atmospheric boundary layer. J Atmos Sci 2005;63:526–46.

[36] Kristensson E, Berrocal E, Alden M. Extinction coefficient imaging of turbid media using dual structured laser illumination planar imaging. Opt Lett 2011;36(9):1656–8.

[37] Lafaurie B, Nardone C, Scardovelli R, Zaleski G. Modeling merging and fragmentation in multiphase flows with SURFER. J Comput Phys 1994;113:134–47.

[38] Le Chenadec V, Pitsch H. A 3d unsplit forward/backward volume-of-fluid approach and coupling to the level set method. J Comput Phys 2013;233:10–33.

[39] Lebas R, Menard R, Beau P, Berlemont A, Demoulin F. Numerical simulation of primary break-up and atomization: DNS and modelling study. Int J Multiphase Flow 2009;39:247–60.

[40] Lessani B, Papalexandris M. Time-accurate calculation of variable density flows with strong temperature gradients and combustion. J Comput Physics 2006;212:218–46.

[41] Lewis P, Shedler G. Simulation of nonhomogeneous poisson processes by thinning.. Nav Res Log 1979;26(3):403–13.

[42] Lilly DK. A proposed modification of the germano subgrid-scale closure method. Phys Fluids A 1992;4(3):633–5.

[43] Linne M. Imaging in the optically dense regions of a spray: A review of developing techniques. Prog Energy Combust Sci 2013;39(5):403–40.

[44] Lörstad D.. Numerical modeling of deforming bubble transport related to cavitating hydraulic turbines. 2003. PhD Thesis

[45] Lörstad D, Francois M, Shyy W, Fuchs L. Volume of fluid and immersed boundary investigations of a single rising droplet. In: AIAA, 41st aerospace science meeting and exibition; 2003. p. 1282.

[46] Lörstad D, Francois M, Shyy W, Fuchs L. Assessment of volume of fluid and immersed boundary methods for droplet computations. Int J Num Meth Fluids 2004;46:109–25.

[47] Lörstad D, Fuchs L. High order surface tension VOF-model for 3d bubbly flows with high density ratio. J Comput Phys 2004;200:153–76.

[48] Martínez-Martínez S, Sánchez-Cruz F, Riesco-Ávila J, Gallegos-Muñoz A, Aceves S. Liquid penetration length in direct diesel fuel injection. Appl Therm Eng 2008;28(14–15):1756–62.

[49] Meier M, Yadigaroglu G, Smith B. A novel technique for including surface tension in PLIC-VOF methods. Eur J Mech B/Fluids 2002;21:61–73.

[50] Menard T, Tanguy S, Berlemont A. Coupling level set/VOF/ghost fluid methods: Validation and application to 3d simulation of the primary break-up of a liquid jet. Int J Multiphase Flow 2006;33:510–24.

[51] Movaghar A, Linne M, Oevermann M, Meiselbach F, Schmidt H, Kerstein AR. Numerical study of liquid breakup at the surface of turbulent liquid jets using one-dimensional turbulence. ILASS - Europe 2014, 26th annual conference on liquid atomization and spray systems, 8–10 Sep. 2014, Bremen, Germany; 2014.

[52] Noh W, Woodward P. SLIC (Simple Line Interface Calculation). Lect Notes in Phys 1976;59:330–40.

[53] Osher S, Sethian J. Fronts propagating with curvature-dependent speed: Algorithms based on hamilton-jacobi formulations. J Comput Phys 1988;79:234–46.

[54] Panton R. Incompressible flow. New York: John Wiley & Sons; 1996.

[55] Pope S. Turbulent flows. New York: Cambridge University Press; 2000.

[56] Popinet S. An adaptive solver for surface-tension-driven interfacial flows. J Comput Phys 2009;228:5838–66.

[57] Puckett E, Almgren A, Bell J, Marcus D, Richter W. A high-order projection method for tracking fluid interfaces in variable density incompressible flows. J Comput Phys 1997;130:269–82.

[58] Reitz R, Bracco F. Mechanism of atomization of liquid jets. Phys Fluids 1982;25:1730–42.

[59] Renardy Y, Renardy M. Prost: a parabolic reconstruction of surface tension for the volume of fluid method. J Comput Phys 2002;183:400–21.

[60] Roache P. Quantification of uncertainty in computational fluid dynamics. Ann Rev Fluid Mech 1997;29:123–60.

[61] Rudman M. Volume-tracking methods for interfacial flow calculations. Int J Num Meth Fluids 1997;24:671–91.

[62] Rudman M. A volume-tracking method for incompressible multifluid flows with large density variations. Int J Num Meth Fluids 1998;28:357–78.

[63] Sagaut P. Large eddy simulation for incompressible flows: An introduction. 2nd edition. Berlin and Heidelberg: Springer; 2004.

[64] Sethian J. A fast marching level-set method for monotonically advancing fronts. Proc Natl Acad Sci USA 1996;93. 1591–95

[65] Shinjo J, Umemura A. Simulation of liquid jet primary breakup: Dynamics of ligament and droplet formation. Int J Multiphase Flow 2010;36:513–32.

[66] Shinjo J, Umemura A. Detailed simulation of primary atomization mechanisms in diesel jet sprays (isolated identification of liquid jet tip effects). Proc Combust Inst 2011;33:2089–97.

[67] Shinjo J, Umemura A. Surface instability and primary atomization characteristics of straight liquid jet sprays. Int J Multiphase Flow 2011;37:1294–304.

[68] Siamas GA, Jiang X, Wrobel LC. Direct numerical simulation of the near-field dynamics of annular gas-liquid two-phase jets. Phys Fluids 2009;21(042103):1–14.

[69] Sirignano W, Mehring C. Review of throry of distortion and disintegration of liquid streams. Prog Energy Combust Sci 2000;26:609–55.

[70] Smagorinsky J. General circulation experiments with the primitive equations: I. the basic equations. Mon Weather Rev 1963;91:99–164.

[71] Som S, Aggarwal S, El-Hannouny E, Longman D. Investigation of nozzle flow and cavitation characteristics in a diesel injector. J Eng Gas Turbines Power 2010;132(4):042802.

[72] Suh H-K, Lee C. Effect of cavitation in nozzle orifice on the diesel fuel atomization characteristics. Int J Heat Mass Transfer 2008;29:1001–9.

[73] Ubbink O.. Numerical prediction of two fluid systems with sharp interfaces. 1997. PhD Thesis

[74] Unverdi S, Tryggvarson G. A front tracking method for viscous incompressible multi-fluid flows. J Comput Phys 1992;100:25–37.

[75] van Wachem B, Schouten J. Experimental validation of a 3-d lagrangian VOF model: Bubble shape and rise velocity. AIChE J 2002;48(12):2744–53.

[76] Varde K, Popa D, Varde L. Spray angle and atomization in diesel sprays. SAE Tech Pap 1984. 841055

[77] Williams M, Kothe D, Puckett E. Accuracy and Convergence of Continuum Surface-Tension Models. In: Shyy W, Narayanan R, editors. Fluid dynamics at interfaces. Cambridge university Press; 1999. p. 295–305.

[78] Xiao F, Dianat M, McGuirk J. LES of turbulent liquid jet primary breakup in turbulent coaxial air flow. Int J Multiphase Flow 2014;60:103–18.

[79] Young D. Time-dependent multi-material flow with large fluid distortion. Num Meth Fluid Dyn 1982:273–85.

[80] Yuan W, Schnerr GH. Numerical simulation of two-phase flow in injection nozzles: Interaction of cavitation and external jet formation. J Fluids Eng 2003;125(6):963–9.